The Cryptophycin−Tubulin Ring Structure Indicates Two Points of Curvature in the Tubulin Dimer†

Norman R. Watts,‡,§ Naiqian Cheng,§ Wendy West,|| Alasdair C. Steven,§ and Dan L. Sackett*,||

Protein Expression Laboratory and Laboratory of Structural Biology Research, National Institute of Arthritis and Musculoskeletal and Skin Diseases, and Laboratory of Integrative and Medical Biophysics, National Institute of Child Health and Human Development, National Institutes of Health, Bethesda, Maryland 20892

Received June 24, 2002; Revised Manuscript Received August 19, 2002

ABSTRACT: Cryptophycin-1 is the parent compound of a group of cyclic peptides with potent antineoplastic activity. Cryptophycins are thought to function by modulating the dynamic instability of spindle microtubules, and in vitro are known to bind in an equimolar ratio to the β-tubulin subunit and to induce the formation of ring-like complexes. However, the detailed mechanisms whereby the cryptophycins interact with tubulin are not known. We have investigated the origin of the conformational changes in tubulin both biochemically and by electron microscopy and image analysis. Cryptophycin was found to protect both α- and β-tubulin against proteolysis by trypsin, indicating conformational changes in specific regions of both subunits. The ring mass was determined to be ∼0.81 MDa by sedimentation velocity combined with dynamic light scattering and by STEM, indicating a complex of eight $\alpha\beta$ dimers. Statistical analysis of rings imaged by cryoelectron microscopy revealed 16-fold symmetry, corresponding to eight dimers. Computational averaging based on this symmetry yielded an image of a 24 nm diameter ring, at 2.6 nm resolution, that clearly distinguishes intradimer contacts from interdimer contacts, and allows discrimination of α-subunits from β-subunits. Fitting of the tubulin dimer crystal structure into this projected density map indicates two points of curvature: a 13° intradimer bend and a 32° interdimer bend. We conclude that drug binding to one subunit (β) results in two bends per dimer, affecting both subunits.

Tubulin is the principal protein of microtubules (MT),[1] but has the interesting capacity to form a number of other, non-MT, polymers. Even MT are not a uniquely defined structure, but can have different forms. In addition to the common single 13-protofilament polymer, tubulin is known to occur in MT with other protofilament numbers, as well as in doublet and triplet MT (as in axonemes and basal bodies), and other configurations. For a review, see ref *1*.

Non-MT polymers of tubulin are often formed following binding of one of the many small molecules that are known to interact with the tubulin dimer. These include the natural allosteric ligands, the guanine nucleotides. The tubulin dimer assumes different conformations depending on the phosphorylation state of the guanine nucleotide bound to the β-subunit. The tubulin dimer with GTP bound in the β-subunit adopts a straight conformation that is able to assemble into linear $\alpha\beta\alpha\beta$... polymers (protofilaments) that comprise the wall of the MT. The GTP is hydrolyzed after incorporation into the lattice of the MT polymer, meaning that the bulk of the MT is composed of GDP-bound tubulin. GDP-bound tubulin preferentially adopts a bent $\alpha-\beta$ configuration, resulting in curved $\alpha\beta\alpha\beta$... protofilaments. These curved protofilaments appear to break off from the ends of the MT lattice to form double-nested rings with an average diameter of ∼48 nm (*2*). Cryoelectron microscopy studies have demonstrated that GDP−tubulin rings occur in multiple different sizes and forms, including nested doublets with outer rings of 14, 15, or 16 dimers (*3*).

Both literature and intuition suggest that the curvature results from changes in the β-subunit, because this is the one that binds the nucleotide that undergoes a change in phosphorylation status. The structure of the tubulin dimer, as revealed by electron crystallography (*4*), shows the exchangeable nucleotide site (E-site) on β-tubulin to be exposed on the outer surface of the dimer (as opposed to the nonexchangeable N-site on α-tubulin) and on the (+)-end of the MT protofilament. It has been suggested (*3*, *5*, *6*) that the structural change induced by hydrolysis of GTP to GDP on the β-subunit results in an intradimer change in conformation (presumably an intra-β change), rather than a change in α-tubulin, or a change in interdimer contacts. The detailed origin of the change in curvature is, however, not known because there are as yet no high-resolution structures for tubulin rings.

† N.R.W. was supported in part by the NIH Intramural AIDS Targeted Antiviral Program.

* To whom correspondence should be addressed: National Institutes of Health, Bldg. 12A, Rm. 2041, Bethesda, MD 20892-5626. Telephone: (301) 594-0358. Fax: (301) 496-2172. E-mail: sackettd@mail.nih.gov.

‡ Protein Expression Laboratory, National Institute of Arthritis and Musculoskeletal and Skin Diseases.

§ Laboratory of Structural Biology Research, National Institute of Arthritis and Musculoskeletal and Skin Diseases.

|| National Institute of Child Health and Human Development.

[1] Abbreviations: CTF, contrast transfer function; EGTA, ethylene glycol bis(β-aminoethyl ether)-*N*,*N*,*N*′,*N*′-tetraacetic acid; GDP, guanosine 5′-diphosphate; GTP, guanosine 5′-triphosphate; MT, microtubules; SD, standard deviation; SEM, standard error of the mean; STEM, scanning transmission electron microscopy.

10.1021/bi020430x
Published on Web 09/28/2002

A large and diverse group of natural and synthetic small molecules are known that disrupt MT polymers and poison mitosis, notably, drugs that bind to sites named for colchicine or vinblastine. For a review, see ref *7*. Many but not all of these compounds induce formation of aberrant polymers. Vinca alkaloids and a number of other agents bind to β-tubulin in a region near the E-site that has been termed the "vinca domain" (*8*). This region includes the binding site for the vinca alkaloids per se and their competitive inhibitors such as maytansine and rhizoxin. In addition, there is an overlapping binding surface that is the focus of interaction for a number of tubulin-binding peptides. These natural product peptides and depsipeptides are tri- and tetrapeptide structures, both linear and cyclic, and are typified by cryptophycin, dolastatin, and hemiasterlin (*9*). These compounds all have the ability to prevent MT polymerization, resulting not in the simple polymerization inhibition seen with other compounds such as the colchicine site ligand podophyllotoxin but instead in the formation of ring-like polymers of tubulin (*8*, *10*).

These compounds are among the most potent antimitotic agents known, with cytotoxic IC_{50} values in the picomolar range (*8*). They are competitive inhibitors of each other, noncompetitive inhibitors of vinblastine binding, and without effect on colchicine binding. Their common binding site has been termed the "peptide site" of the vinca domain (*8*, *11*) and is probably located on β-tubulin near the E-site (*12*). They have in common the properties of being similarly sized hydrophobic peptides that bind to tubulin with a 1:1 stoichiometry per tubulin heterodimer. In addition, they share the ability to induce single-protofilament ring polymers of tubulin, distinct from the nested-doublet rings formed with GDP, and the stacked-doublet rings coassembled with HIV-Rev (*13*).

However, the peptide-induced rings differ from each other in their structural details. The clearest example of these differences is that provided by the cryptophycin−tubulin rings (*9*). Having diameters of approximately 24 nm, these rings are significantly smaller than the GDP-, dolastatin-, or hemiasterlin-induced rings which have diameters of >40 nm (*9*). Hence, the curvature of the dimers is greater in these rings than in the other cases. Cryptophycin−tubulin rings may therefore provide an unusually clear substrate on which to investigate the question of how curvature is induced in linear polymers of tubulin dimers; is it primarily an intradimer effect induced in β-tubulin, as proposed for GDP−tubulin rings (*5*), or are changes also induced in α-tubulin, or in the dimer−dimer contact? To address these questions, we have examined the drug−tubulin complexes both biochemically and by cryoelectron microscopy and computational image analysis.

MATERIALS AND METHODS

Materials. Tubulin was isolated from rat brain microtubule protein (*14*) by differential polymerization as described previously (*15*). Tubulin stock solutions were prepared at 25 mg/mL in MME buffer [100 mM MES, 1 mM $MgCl_2$, and 1 mM EGTA (pH 6.9)], drop-frozen in liquid nitrogen, and stored at −80 °C.

Cryptophycin-1 was a kind gift from S. Mooberry (Cancer Research Center of Hawaii, Honolulu, HI). Dolastatin-10 was provided by R. Schultz (Drug Synthesis and Chemistry Branch, National Cancer Institute, National Institutes of Health). Other reagents and enzymes were obtained from Sigma-Aldrich Chemical Co. (St. Louis, MO).

Formation of Cryptophycin−Tubulin Complexes. Tubulin and Cryptophycin-1 were diluted with MME buffer to give final concentrations of 2.5 μM tubulin and 3.75 μM cryptophycin (or others as indicated), and then incubated for 30 min at room temperature. Dolastatin-10 complexes were formed in a similar fashion.

Proteolysis of Tubulin. The effects of drug binding on tubulin conformation were monitored by partial proteolysis as described previously (*16*). Tubulin at 10 μM in MME was incubated for 20 min at room temperature with 20 μM drug additions as indicated. Proteolysis was then performed with trypsin, chymotrypsin, or subtilisin. Trypsin or chymotrypsin was added in a 1:40 ratio by weight to tubulin (enzyme final concentration of approximately 1 μM). The reaction mixture was immediately transferred to an ice bath and maintained for 30 min. Leupeptin was added to a final concentration of 50 μM to stop the trypsin reaction, while phenylmethanesulfonyl fluoride was added to a final concentration of 2.5 mM to stop the chymotrypsin reaction. The subtilisin reaction was carried out with enzyme added at a 1:50 ratio by weight to tubulin, and the reaction was allowed to proceed for 30 min at 22 °C. The reaction was stoppped with 2.5 mM phenylmethanesulfonyl fluoride. The samples were then processed for SDS gel electrophoresis on NuPage 4−12% gels (Invitrogen-Novex, Carlsbad, CA).

Analytical Ultracentrifugation and Dynamic Light Scattering. Cryptophycin−tubulin ring polymers were analyzed by sedimentation velocity and dynamic light scattering. Sedimentation velocity data were recorded at 20 °C using a Beckman XLA analytical ultracentrifuge (Beckman Coulter, Fullerton, CA) equipped with absorption optics. Sedimentation coefficients were derived using software provided by Beckman Coulter. Dynamic light scattering analysis was performed using a Brookhaven Instruments Corp. (Holtsville, NY) laser light scattering spectrometer equipped with an argon ion laser and a BI2030AT digital correlator. Diffusion coefficients were obtained using software provided by Brookhaven Instruments.

Scanning Transmission Electron Microscopy and Mass Analysis. Specimens were applied to titanium grids bearing prewetted thin carbon films, washed 10 times by serial transfer on drops of 20 mM ammonium acetate, blotted to a thin film, frozen in liquid nitrogen, and allowed to dry for 6−8 h at a constant sublimation rate. Tobacco mosaic virus particles were included as internal mass standards (131.4 kDa/nm). Digital micrographs were recorded in the dark-field mode of the Brookhaven STEM at 1.0 nm/pixel (*17*).

Mass determinations of rings were made by interactive analysis of the STEM micrographs using PIC programs (*18*). Cryptophycin−tubulin rings were prone to breakage during grid preparation; consequently, only a total of 55 well-preserved particles were measured. Dolastatin−tubulin rings were even more fragile and frequently tended to undergo ring opening and fragmentation; therefore, mass-per-unit-length measurements were taken. A total of 55 particles were measured.

Electron Microscopy. Specimens for cryoelectron microscopy were applied to copper grids bearing continuous thin

carbon films, blotted, and frozen in liquid nitrogen-cooled liquid ethane using a Reichert KF80 cryofixation device (Leica AG, Vienna, Austria). Continuous carbon films were used because it was found that the rings adsorbed to carbon and were consequently depleted from the holes in fenestrated films. Specimens were visualized with a CM200-FEG electron microscope (FEI, Mahwah, NJ) fitted with a model 626 cryoholder (Gatan, Pleasanton, CA) and operating at 120 kV. Micrographs were recorded at 38000× magnification and 3.1−3.6 μm defocus under low-dose conditions (*19*). Specimens negatively stained with uranyl acetate were examined with a Zeiss EM 902 electron microscope at 30000× magnification (Carl Zeiss, Thornwood, NY). Magnifications were calibrated with reference to the 4.0 nm axial spacing of MT (*20*) as measured by Fourier analysis of micrographs.

Image Processing. Cryoelectron micrographs, previously determined by optical diffraction to be well-stigmated and free of drift, were digitized on a SCAI densitometer (Z/I Imaging, Huntsville, AL) at 0.37 nm/pixel. The positions of the first zeros in the contrast transfer functions (CTF) ranged from $(3.2\ \text{nm})^{-1}$ to $(3.5\ \text{nm})^{-1}$. Micrographs were corrected for CTF effects using CTFMIX (*21*, *22*). Particles were preprocessed (extracted, normalized, and corrected for background gradients) in a semiautomatic fashion using the program X3D (*21*) and then processed further with PIC (*18*). Briefly, 577 rings were translationally centered by cross correlation and then analyzed for the presence of rotational symmetries using FULLROTASTAT, a refined version of the program originally described by Kocsis et al. (*23*). Sixteen-fold symmetry was found to be statistically significant in the radial zone that encloses the tubulin ring. This is in fact a pseudosymmetry because the strong low-resolution signal does not discriminate between α- and β-subunits; the true symmetry is 8-fold (see the Results). The rings with the strongest 16-fold symmetry were each 8-fold symmetrized and then subjected to two cycles of correlation alignment for orientation and origin. In principle, the rings could have adsorbed to the carbon support film with either face in contact with it. These two modes of attachment produce the same projection image, but with opposite hands. The data were made consistent in this respect by in each case selecting the enantiomer that gave the higher correlation with the current reference image. The OMO algorithm was used to remove outliers, prior to averaging (*24*). The final average image, including 228 particles, had a resolution of 2.6 nm (*25*). To determine the intradimer curvature, the tubulin heterodimer (PDB entry 1JFF) and the individual α- and β-subunits were modeled into the projected electron density map using the program O (*26*).

RESULTS

To investigate the cryptophycin−tubulin ring polymers, we first examine the biochemical evidence for structural change induced in tubulin by cryptophycin binding. We then characterize the rings structurally and analyze in detail the points of curvature.

Limited Proteolysis. The conformation of tubulin in the cryptophycin ring polymers was initially probed by limited proteolysis. Tubulin is relatively resistant to proteolysis, but a few sites on the protein are cleaved by proteases. These

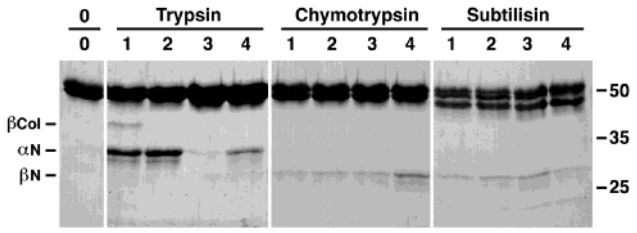

FIGURE 1: Tubulin conformation probed by protease digestion. Tubulin−drug complexes were probed by proteolysis and separated by SDS gel electrophoresis as described in Materials and Methods. Samples were probed with no enzyme (0), trypsin, chymotrypsin, or subtilisin. Enzyme-digested samples contained no drug (lane 1), rhizoxin (lane 2), Cryptophycin-1 (lane 3), or Dolastatin-10 (lane 4). The location of molecular mass markers of 50, 35, and 25 kDa are denoted on the right, top to bottom. The location of the band produced by tryptic cleavage of β-tubulin after K392 is indicated by βCol. The amino-terminal fragments produced by tryptic cleavage of α-tubulin and chymotryptic cleavage of β-tubulin are denoted by αN and βN, respectively.

cleavage sites are differentially affected by drug binding, local conformational changes, and changes in association state (reviewed in ref *27*). Figure 1 shows the results of proteolytic cleavage of tubulin by trypsin, chymotrypsin, and subtilisin, following incubation with no drug (lane 1), rhizoxin (lane 2), cryptophycin (lane 3), or dolastatin (lane 4). We will first focus on the results with trypsin, and then examine the results with the other two enzymes. Trypsin is known to cleave the native tubulin dimer at two sites: after αR339 and after βK392 (*2*, *16*, *28*). Both sites are located on the face of the tubulin dimer exposed on the outer surface of microtubules. As shown (Figure 1), both cleavages are prevented by cryptophycin ring formation. Binding of rhizoxin to the vinca site is sufficient to prevent the β-cleavage but does not alter the α-cleavage. Dolastatin ring formation or vinblastine spiral formation (data not shown) additionally reduces the extent of α-cleavage, but only cryptophycin eliminates both. In contrast to the results with trypsin, chymotrypsin cleavage of β-tubulin after βY281 is little altered by cryptophycin, although it is enhanced by dolastatin. Subtilisin cleavage of a small acidic carboxyl-terminal peptide from both subunits, reducing their mass by ∼2 kDa, is also little altered by cryptophycin binding. Cryptophycin thus appears to alter the conformation of particular regions of α- as well as β-tubulin, while having little effect on nearby regions of the β-subunit, or the carboxyl-terminal regions of both subunits.

Analytical Ultracentrifugation and Dynamic Light Scattering. Rings were analyzed by analytical ultracentrifugation and dynamic light scattering to determine their mass. The results are presented in Table 1 for cryptophycin−tubulin rings and, for comparison, dolastatin−tubulin rings. The sedimentation velocity of the cryptophycin−tubulin rings indicated a homogeneous population of 15S particles, while dynamic light scattering yielded a diffusion coefficient of $1.8 \times 10^{-7}\ \text{cm}^2\ \text{s}^{-1}$. Combining these yielded a ring mass of 0.77 MDa, indicating a ring of eight tubulin heterodimers (100 kDa each). Attempts to obtain a ring mass by equilibrium ultracentrifugation were not successful due to continual upward drift in apparent molecular mass during the long equilibrium times required for a particle of this size. The need for short run times due to tubulin decay has been noted previously (*29*).

Table 1: Structural Characteristics of Peptide−Tubulin Rings

	microscopy				centrifugation and light scattering			
complex[a]	diameter[b] (nm)	width[c] (nm)	mass/length[d] (kDa/nm)	mass[e] (MDa)	sedimentation coefficient (S)	diffusion coefficient ($\times 10^7$ cm^2 s^{-1})	mass[f] (MDa)	no. of dimers
Cryptophycin-1	23.8 ± 0.09, 228	6.3 ± 0.17, 228	11	0.80 ± 0.01, 55	15	1.8	0.77	8
Dolastatin-10	44.6 ± 0.2, 41	5.2 ± 0.06, 41	12.9 ± 0.3, 55	ND	20	1.3	1.4	14

[a] Drug used to induce tubulin rings. [b] Diameter of the ring, as determined between peak maxima, of cross sections of azimuthally averaged rings. Cryptophycin rings in vitreous buffer and dolastatin rings in negative stain. Mean ± SEM, number of particles. [c] Width of ring, as determined at the level of the background, of cross sections of azimuthally averaged rings. Cryptophycin rings in vitreous buffer and dolastatin rings in negative stain. Mean ± SEM, number of particles. [d] Mass-per-unit-length, as determined by STEM. For cryptophycin, the value was calculated from the mean diameter and mean mass values of rings. For dolastatin, the value was measured on rings that had opened. Mean ± SEM, number of particles. [e] Mass, as determined by STEM. Values for dolastatin−tubulin rings were not determined due to fragmentation of particles (but see footnote d). Mean ± SEM, number of particles. [f] Mass, as calculated from sedimentation and diffusion coefficients with the Svedberg equation $M = sRT/D(1 - \bar{v}\rho)$. $\bar{v}$ was taken to be 0.736, and $\rho = 1$.

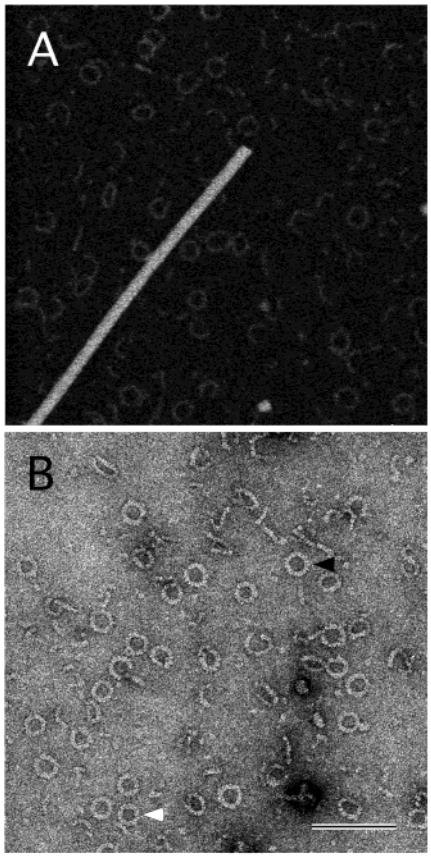

FIGURE 2: Cryptophycin−tubulin rings visualized by STEM and negative stain electron microscopy. (A) Cryptophycin−tubulin rings prepared by freeze-drying and visualized by STEM. Analysis of the rings gives a value of 0.81 ± 0.01 MDa (mean ± SEM). The long bright object is a TMV virion serving as an internal mass standard (131.4 kDa/nm). (B) Cryptophycin−tubulin rings as visualized by negative staining with uranyl acetate. Some of the particles show angularity at a few points (open arrowhead). Distinct subunits are visible at the edges of some particles (filled arrowhead). The bar is 100 nm long.

STEM and Mass Analysis. The cryptophycin−tubulin rings were also analyzed by STEM to determine their mass. The rings were more disrupted by freeze-drying during preparation for STEM than when supported by negative stain (below), frequently breaking open and fragmenting (Figure 2A). Cryptophycin−tubulin rings were, however, somewhat more stable than dolastatin−tubulin rings observed under the same conditions (not shown). As in negative stain, the rings show some size heterogeneity (Figure 2 and Table 1). STEM mass analysis gives a value of 0.81 ± 0.09 (SD) [±0.01 (SEM)] MDa for each ring. This result, although obtained from a limited data set, is very similar to that obtained by analytical ultracentrifugation and dynamic light scattering and is consistent with a complex of eight $\alpha\beta$ tubulin heterodimers. Analysis of dolastatin−tubulin rings, by comparison, indicated a ring composed of 14 heterodimers, consistent with previous results (*13*). The mass-per-unit-length values, for both cryptophycin− and dolastatin−tubulin rings, are close to 12.5 kDa/nm, as expected for a single tubulin protofilament (Table 1).

Negative Stain Electron Microscopy. The induction of tubulin rings by cryptophycin was monitored by negative stain electron microscopy (Figure 2B). The rings were stable and showed little breakage during grid preparation. They also appear to be relatively round, and although some show angularity, this is not consistent from particle to particle. None of them appear to be octagonal. The rings appear to be single; i.e., they are neither nested nor stacked double rings as is sometimes observed in other instances (*5*), although no definitive side views were observed to confirm the latter. The STEM data and analytical ultracentrifugation results (above) and the symmetry analysis (below) indicate that the rings are in fact single, i.e., not stacked. The rings appear to be slightly heterogeneous in diameter but uniform in thickness (see also Table 1). Distinct subunits can be observed at the edges of some particles.

Cryoelectron Microscopy and Symmetry Analysis. To pursue the possibility of two cryptophycin-induced conformational changes in the tubulin heterodimer, as suggested by the limited proteolysis results, we analyzed the rings by cryoelectron microscopy and computational image analysis. The initial attempts to visualize cryptophycin−tubulin rings by cryoelectron microscopy using holey carbon films failed when the particles could not be located within the fenestrations. Use of continuous carbon films circumvented this difficulty but at the cost of introducing a higher level of noise into the images. Micrographs were selected that showed numerous well-contrasted ice-embedded particles (Figure 4A), and these data were corrected for phase contrast transfer function (CTF) effects (*21*, *22*). Particles ($n = 577$) were preprocessed and then analyzed for the presence of rotational symmetries. To determine the symmetries of the complexes quantitatively, we employed a statistical procedure for rotational symmetry detection that has been described in detail previously (*13*, *23*). In essence, the procedure involves

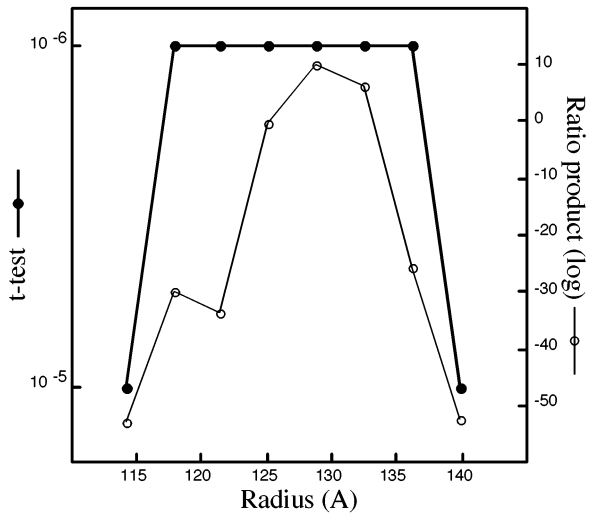

FIGURE 3: Detection of 16-fold symmetry in cryoelectron micrographs of cryptophycin−tubulin rings. Two statistical measures of significance were employed to determine the presence of rotational symmetries in rings (*23*). The Student's *t* test assesses, at each radius, which orders of symmetry are significantly represented in the population. The vertical scale represents the probability that the symmetry in question could have arisen at random. For this data set, only 16-fold symmetry was significantly above a threshold of $P < 10^{-4}$ (●). The program does not calculate probabilities smaller than 10^{-6}, so the plotted probabilities are truncated at this value between radii of ∼120 and 140 Å. The spectral ratio product [SPR (○)] is calculated as follows for each symmetry and each radius. Each image is represented by the ratio between the amplitude of the corresponding term of its Fourier transform (in polar coordinates) and the corresponding mean amplitude for background images; these ratios are multiplied together. The resulting product rapidly approaches zero as the number of particles increases, except when a symmetry is present. In essence, the *t* test shows if a given symmetry is statistically significant and over what radial range, while the SPR shows where that symmetry is most strongly expressed. In this analysis, 16-fold symmetry was the only harmonic detected as being significant, peaking at radii of ∼125−135 Å, in the middle of the ring wall.

the calculation of two statistical measures to determine the significance of all symmetries present at all radii for the full data set by comparison with the corresponding signals from a reference set of background images. Multiple rotational symmetries can be detected, provided they are sufficiently represented *in the population*.

Sixteen-fold symmetry was found to be statistically significant, as determined by the *t* test, and it was maximal in the radial position corresponding to the middle of the tubulin ring, as shown by the ratio product (Figure 3). Individual particles exhibiting 16-fold symmetry were further screened visually to eliminate those affected by distortion or contamination (Figure 4B). These particles were then 8-fold symmetrized, subjected to two cycles of translational and rotational alignment according to handedness, and finally averaged (see Materials and Methods). By applying 8-fold symmetry to the individual 16-fold symmetric particles (a valid operation because they are composed of heterodimers) prior to aligning them, we were able to improve their registration. The program OMO (*24*) was used to remove outliers before a final average was calculated from 228 particles (Figure 4C).

The resulting image shows eight bilobed densities uniformly arranged in a ring. The two lobes within each such density are assumed to be α- and β-tubulin subunits. The region between the presumptive heterodimers is less dense than within the dimers, and occurs at a slightly lower radius (Figure 4C,D). The serrated appearance of the periphery of the map suggests that the side of the dimer normally facing the inside of the MT is now on the outside of the ring, as has been proposed for GDP−tubulin rings (*3*). Consequently, the heterodimer is being viewed from the side, i.e., as seen from the adjacent protofilament. The polarity of the serrations, as depicted in panels C and D of Figure 4, suggests that the β-subunit is the one on the left in each dimer, analogous to the stathmin−tubulin complex (*30*). Also, the subunits within each dimer have a slightly different density distribution, with that of the one on the right, and presumably the α-subunit, being more dispersed (this is best observed when interactively adjusting the contrast). The corresponding projected density distribution of the tubulin dimer, calculated from the atomic coordinates (PDB entry 1JFF) with B-soft (*31*), also shows that the density of the α-subunit is more dispersed, supporting the above assignment. It should be noted that the 26 Å resolution attained here would normally not be sufficient to discriminate between α- and β-subunits, were they for example in a linear polymer; however, the high curvature inherent in these rings accentuates the difference between intra- and interdimer contacts, allowing subunit identification even in the case of limited resolution.

Given a uniform ring composed of eight dimers, there must be 45° of curvature per dimer, with this occurring either between dimers, within dimers, or both. Visual inspection suggests that at least some of the curvature is occurring within the dimer. To determine the degree of intradimer curvature, tubulin was modeled into the electron density map both as a "straight" dimer (PDB entry 1JFF) and as individual α- and β-subunits using O (*26*) with the β-subunit on the left and the C-terminal helix of each subunit facing toward the inside of the ring (Figure 4E). All rotations were in the plane of the ring. Compared to the straight conformation, there are 13° of curvature between the α- and β-subunits, and therefore 32° between heterodimers.

DISCUSSION

Switching between conformational states is a common means of regulating biological activity. Such conformational shifts are often regulated by the phosphorylation status of bound guanine nucleotide (*32*). Altering, exaggerating, or preventing these conformational shifts affords a mechanism by which added drugs can alter biological processes. All of these events occur in the tubulin−MT system, in which the switch from bound GTP to GDP converts the tubulin heterodimer from a straight, MT-polymerization-competent form to a "bent" form that cannot polymerize into MT but can form various other curved polymers. Many antimitotic drugs can induce curved polymers of tubulin, in particular, vinca domain-binding drugs. Hence, understanding the structural origins of curvature in these polymers is important to understanding the regulation of MT function and the action of many antimitotic drugs. We have chosen to study the ring polymers induced by Cryptophycin-1 because these rings have the highest curvature of known tubulin polymers. We wished to determine whether curvature originated in a single region of the tubulin heterodimer, near the E-site and the presumed vinca binding site, or if there is more than one point of curvature.

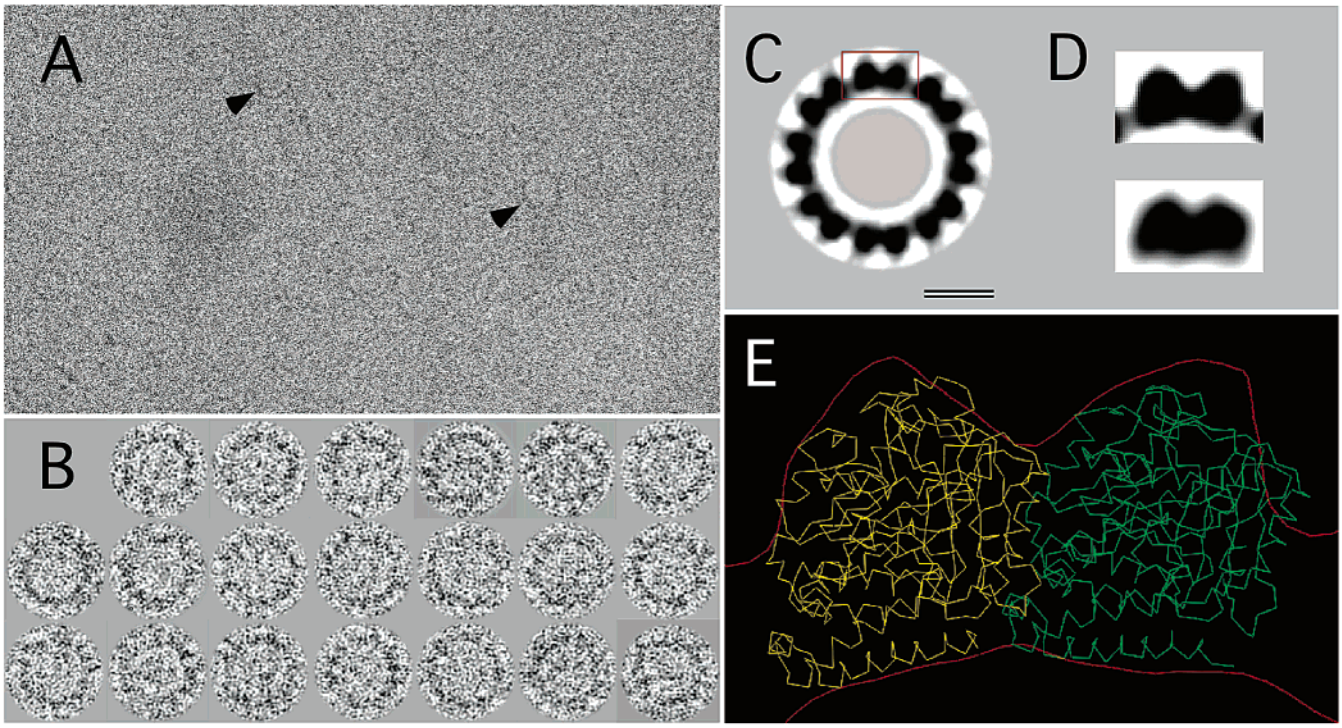

FIGURE 4: Cryptophycin−tubulin rings visualized by cryoelectron microscopy and image processing. (A) Field of particles preserved in a film of vitreous buffer on a thin continuous carbon film. Distinct subunits are visible at the edges of some particles (filled arrowheads). (B) Two-fold enlargements of particles such as those seen in panel A. (C) Cross-correlation average image of particles previously 8-fold symmetrized (bar is 10 nm long). (D) Comparison of the projection of a curved dimer (upper), cropped from panel C, compared with a similar projection of a straight dimer (lower) calculated from the published atomic coordinates for tubulin (PDB entry 1JFF). (E) Fitting of the α- and *β*-tubulin subunits into the projected cryo-EM envelope of the ring.

It has been argued that the bent form of the dimer is the low-energy form of GDP-bound tubulin (*5*), and the origins of the bend have been discussed (*3*, *6*). Because only the *β*-tubulin G-binding site can be in GTP or GDP forms, it has been suggested that this is the site of structural change that results in a bent form of the dimer and in curved polymers, like the nested doublet GDP ring polymers. These have been shown to have considerable flexibility in diameter and hence in curvature (*3*). Therefore, it might be proposed that drugs that bind near the *β* E-site and which induce formation of curved polymers do so by altering the extent of curvature induced in a region of the protein already responsible for induction of curvature. Alternatively, the drugs might alter the conformation of a second site, leading to two sites of curvature, presumably due to conformational changes at the (single) binding site propagating through the dimer. Indeed, evidence for two sites of curvature has been reported in the stathmin−tubulin complex (*30*). The cryptophycin−tubulin rings provide an attractive model for examining this question because they are single-filament polymers and contain only eight dimers in the ring (Table 1). Thus, the problem becomes distinguishing between a ring with either 8 or 16 points of bending. Our data support the latter model.

Conformation of Tubulin in Cryptophycin Rings As Assayed by Limited Proteolysis. The conformation of the tubulin subunits in the dimer and in the ring form can be compared by probing their susceptibility to proteolysis. Because proteases cleave at several different known sites, the changes in conformation of different regions of the tubulin molecules can be compared. Our results show that there is little cryptophycin-induced alteration of tubulin structure at the regions of cleavage by subtilisin or chymotrypsin. These regions are the extreme carboxy termini of both subunits, and the M-loop near Y281, respectively. In contrast, sites of trypsin cleavage are altered by cryptophycin-induced ring formation.

Trypsin is known to cleave at two sites on the tubulin dimer: after αR339 and after *β*K392 (*16*, *28*). The α-cleavage occurs in the loop between helix 10 and strand 9. The *β*-cleavage, which occurs in the loop between helices 11 and 12, is enhanced by binding of colchicine to the tubulin dimer, apparently due to unfolding of the C-terminal end of helix 11 (*16*). Both cleavage sites are on the face of the tubulin dimer exposed on the outer surface of the microtubule, and are in regions that appear to be involved in subunit contacts in the microtubule. The α-site is involved in lateral interactions with the neighboring protofilament, while the *β*-loop is involved in longitudinal interactions between dimers (*33*). Microtubule polymerization or zinc sheet formation suppresses cleavage at both sites (*28*).

The cleavage of tubulin by trypsin is altered by the binding of vinca site drugs. Vinca site agents bind to *β*-tubulin in a region near the E-site (*8*). This is adjacent to the H11−H12 loop that is the site of tryptic cleavage, and simple occupancy of the vinca site appears to be sufficient to render this loop resistant to cleavage. Thus, rhizoxin, which binds to tubulin dimers and does not induce any polymer formation (*8*), suppresses the cleavage of *β* as well as the vinca agents that do induce polymer formation. Vinblastine and dolastatin, which bind in the same region but do induce curved polymer formation, reduce the level of cleavage of α, as well as

preventing cleavage of β. Only cryptophycin completely suppresses cleavage at both sites. Suppression of the α-cleavage in microtubules or in zinc sheets is due to burial of this site in the lateral interaction between neighboring protofilaments. This may account for the partial suppression of cleavage by vinblastine because vinca spirals may be composed of two laterally associated protofilaments (*34*). However, this cannot be the case for the cryptophycin polymers, because the ring polymer consists of a single filament of tubulin dimers. Simple protofilament formation per se is not sufficient to suppress this cleavage because trypsin cleavage of α is still observed with the single-filament dolastatin ring polymers. However, the extent of cleavage of dolastatin polymers is reduced relative to the control (Figure 1, compare trypsin lanes 1 and 4), and this may reflect occlusion of the cleavage site due to outward curvature of the filament. Complete suppression by cryptophycin could then be due to the greater curvature of the smaller rings. Therefore, the suppression of cleavage of α-tubulin must be due either to a conformational change induced in α-tubulin by the binding to β-tubulin or to protection of this region of α-tubulin by the intrusion of the β-subunit of the neighboring dimer in the curved filament. We believe that the cleavage of α-tubulin must be due to a conformational change induced in α-tubulin by the binding of cryptophycin to β-tubulin.

The proteolysis data indicate that cryptophycin binding does not massively alter the structure of tubulin because no new bands are seen with any of the proteases. Furthermore, some regions of the protein appear to be completely unaffected by binding, because subtilisin and chymotrypsin cleavage are neither enhanced nor inhibited. However, the results do indicate that cryptophycin binding induces changes in at least two regions of the heterodimer: one in the α-subunit and one in the β-subunit. These two sites of conformational change may indicate two points of curvature in the formation of the ring. To examine these possibilities further, we decided to pursue, first, an objective analysis of the symmetry of the rings and, subsequently, an image reconstruction based on this symmetry.

Symmetry Analysis of Cryptophycin Rings by Cryo-EM and Image Analysis. Preliminary analysis of the cryptophycin polymers by negative stain electron microscopy showed them to be generally round. However, in no instance was it possible to confidently ascertain their symmetry by inspection. When the particles were visualized by cryoelectron microscopy, their appearance was considerably more round, suggesting that the particles in solution are probably uniformly circular (Figure 4B) and that some distortion is introduced when they are dried down in stain. The actual symmetry of the particles was, however, still not clear.

To determine the symmetry of the rings, a quantitative, objective statistical procedure was applied to the cryo-EM data (*23*). This procedure can detect multiple rotational symmetries (polymorphism) when present in a population of particles (*35*−*37*). However, the only signal detected with these data was 16-fold symmetry. There is a possibility that there might be a few rings with other symmetries, but if so, they are so few and their signal is so weak that they did not register as significant in this analysis of the population as a whole. The 16-fold signal corresponds to a 4 nm spacing of subunits around the ring and does not discriminate between α- and β-tubulin subunits; as such, it in fact reports a pseudosymmetry. The radial range over which this signal was detected as statistically significant, and where it was strongest, are shown in Figure 3.

On the basis of the assumption that each ring contains eight dimers arranged with consistent polarity, we applied 8-fold symmetry to the individual images. This operation improved their signal-to-noise ratio by a factor of almost 3, which proved to be sufficient to allow the dimers to be aligned consistently with respect to the rotational setting of the rings (i.e., without half-overlap) and handedness by correlational averaging (cf. Figure 4C). This latter operation, combining 228 rings, further improved the signal-to-noise ratio by a factor of ∼15.

The averaged images revealed a ring clearly composed of eight slightly curved heterodimers with a clear distinction between the subunits within each dimer. The subunits within a dimer have a slightly different density distribution, with that of the α-subunit being more dispersed, similar to what has been observed previously for GDP−tubulin double rings (*3*). Because the perimeter of the ring is serrated, we can assume that the outside of the ring corresponds to the side normally facing the inside of the MT (*3*), in which case the β-tubulin subunit in each heterodimer is positioned counterclockwise relative to the α-tubulin subunit when the complex is depicted with the hand shown in panels C and D of Figure 4. The subunits within heterodimers appear to be joined by a region of density at a radius slightly higher than that which exists between dimers. The distance between the centers of mass of the subunits within a dimer is slightly less than that between dimers, approximately 4.3 versus 4.8 nm, respectively. Aside from this difference in spacing, the subunits are uniformly distributed around the ring. The curvature is 13° between subunits within a dimer, and 32° between subunits from adjacent dimers.

Thus, the curvature induced in tubulin by cryptophycin occurs at two sites, but the curvatures at the two sites are unequal in magnitude. The intradimer bend is only slightly increased over the value of 11° reported in the helical stathmin−tubulin complex (*30*). The interdimer bend is significantly increased over the value of 13° found in the stathmin−tubulin complex, and is the main origin of the increased curvature of the cryptophycin rings compared to the GDP rings or the stathmin complex. Kinesin−tubulin (*38*) and Rev−tubulin (*13*) rings have also been described, but in these cases, no intra- or intersubunit angles were reported. Because the interdimer bend is likely near the binding site of the drug, it suggests that small changes in the structure of the drug can have large effects on the conformation of the drug−tubulin complex and the polymers that it forms by altering the detailed interaction with this site. This may be the explanation for the larger rings formed with dolastatin (14 dimers) and for those reported (*10*) with Cryptophycin-52 (9 dimers), a close analogue of the Cryptophycin-1 used in this study. Our preliminary results (not shown) also indicate that biologically active analogues of Cryptophycin-1, structurally similar to Cryptophycin-52, induce ring polymers larger than those described here.

Cryptophycin-1 is the parent compound of a family of potent antimitotic macrolides thought to function by modulating the dynamic instability of spindle microtubules, and currently undergoing clinical evaluation as antiproliferative agents (*39*). However, the mechanisms whereby the cryp-

tophycins interact with tubulin are not known. Taken together, our results suggest that the binding of cryptophycin to tubulin induces two points of curvature per heterodimer; one involving local changes in the β-subunit and a second involving long-range changes that affect the α-subunit. Both conformational changes would be expected to affect MT dynamics.

ACKNOWLEDGMENT

We thank Drs. James Conway, David Belnap, and Benes Trus for providing computer resources and programs. We also thank Drs. Martha Simon and Joe Wall for providing STEM data. The Brookhaven STEM is an NIH Supported Resource Center (Grant P41-RR01777), with additional support provided by the Department of Energy and the Office of Biological and Environmental Research. N.R.W. dedicates this work to the memory of his sister Madelaine who died of breast cancer May 19, 2002.

REFERENCES

1. Unger, E., Bohm, K. J., and Vater, W. (1990) *Electron Microsc. Rev. 3*, 355−395.
2. Diaz, J. F., Pantos, E., Bordas, J., and Andreu, J. M. (1994) *J. Mol. Biol. 238*, 214−223.
3. Nicholson, W. V., Lee, M., Downing, K. H., and Nogales, E. (1999) *Cell Biochem. Biophys. 31*, 175−183.
4. Nogales, E., Wolf, S. G., and Downing, K. H. (1998) *Nature 391*, 199−203.
5. Melki, R., Carlier, M. F., Pantaloni, D., and Timasheff, S. N. (1989) *Biochemistry 28*, 9143−9152.
6. Downing, K. H., and Nogales, E. (1998) *Curr. Opin. Cell Biol. 10*, 16−22.
7. Jordan, A., Hadfield, J. A., Lawrence, N. J., and McGown, A. T. (1998) *Med. Res. Rev. 18*, 259−296.
8. Hamel, E. (1992) *Pharmacol. Ther. 55*, 31−51.
9. Bai, R., Durso, N. A., Sackett, D. L., and Hamel, E. (1999) *Biochemistry 38*, 14302−14310.
10. Barbier, P., Gregoire, C., Devred, F., Sarrazin, M., and Peyrot, V. (2001) *Biochemistry 40*, 13510−13519.
11. Bai, R. L., Schwartz, R. E., Kepler, J. A., Pettit, G. R., and Hamel, E. (1996) *Cancer Res. 56*, 4398−4406.
12. Downing, K. H. (2000) *Annu. Rev. Cell Dev. Biol. 16*, 89−111.
13. Watts, N. R., Sackett, D. L., Ward, R. D., Miller, M. W., Wingfield, P. T., Stahl, S. S., and Steven, A. C. (2000) *J. Cell Biol. 150*, 349−360.
14. Sackett, D. L., Knipling, L., and Wolff, J. (1991) *Protein Expression Purif. 2*, 390−393.
15. Wolff, J., Knipling, L., and Sackett, D. L. (1996) *Biochemistry 35*, 5910−5920.
16. Sackett, D. L., and Varma, J. K. (1993) *Biochemistry 32*, 13560−13565.
17. Wall, J. S., Hainfeld, J. F., and Simon, M. N. (1998) in *Methods in Cell Biology* (Berrios, M., Ed.) pp 139−166, Academic Press, New York.
18. Trus, B. L., Kocsis, E., Conway, J. F., and Steven, A. C. (1996) *J. Struct. Biol. 116*, 61−67.
19. Cheng, N., Conway, J. F., Watts, N. R., Hainfeld, J. F., Joshi, V., Powell, R. D., Stahl, S. J., Wingfield, P. E., and Steven, A. C. (1999) *J. Struct. Biol. 127*, 169−176.
20. Metoz, F., and Wade, R. H. (1997) *J. Struct. Biol. 118*, 128−139.
21. Conway, J. F., and Steven, A. C. (1999) *J. Struct. Biol. 128*, 106−118.
22. Belnap, D. M., Filman, D. J., Trus, B. L., Cheng, N., Booy, F. P., Conway, J. F., Curry, S., Hiremath, C. N., Tsang, S. K., Steven, A. C., and Hogle, J. M. (2000) *J. Virol. 74*, 1342−1354.
23. Kocsis, E., Cerritelli, M. E., Trus, B. L., Cheng, N., and Steven, A. C. (1995) *Ultramicroscopy 60*, 219−228.
24. Unser, M., Steven, A. C., and Trus, B. L. (1986) *Ultramicroscopy 19*, 337−348.
25. Unser, M., Trus, B. L., and Steven, A. C. (1987) *Ultramicroscopy 23*, 39−52.
26. Jones, T. A., Zou, J. Y., Cowan, S. W., and Kjeldgaard, M. (1991) *Acta Crystallogr. A47*, 110−119.
27. Sackett, D. L. (1995) *Biochemistry 34*, 7010−7019.
28. Sackett, D. L., and Wolff, J. (1986) *J. Biol. Chem. 261*, 9070−9076.
29. Sackett, D. L., and Lippoldt, R. E. (1991) *Biochemistry 30*, 3511−3517.
30. Gigant, B., Curmi, P. A., Martin-Barbey, C., Charbaut, E., Lachkar, S., Lebeau, L., Siavoshian, S., Sobel, A., and Knossow, M. (2000) *Cell 102*, 809−816.
31. Heymann, J. B. (2001) *J. Struct. Biol. 133*, 156−169.
32. Vetter, I. R., and Wittinghofer, A. (2001) *Science 294*, 1299−1304.
33. Nogales, E., Whittaker, M., Milligan, R. A., and Downing, K. H. (1999) *Cell 96*, 79−88.
34. Jordan, M. A., Margolis, R. L., Himes, R. H., and Wilson, L. (1986) *J. Mol. Biol. 187*, 61−73.
35. Li, J., Gao, X., Ortega, J., Nazif, T., Joss, L., Bogyo, M., Steven, A. C., and Rechsteiner, M. (2001) *EMBO J. 20*, 3359−3369.
36. Singh, S. K., Rozycki, J., Ortega, J., Ishikawa, T., Lo, J., Steven, A. C., and Maurizi, M. R. (2001) *J. Biol. Chem. 276*, 29420−29429.
37. Ishikawa, T., Beuron, F., Kessel, M., Wickner, S., Maurizi, M. R., and Steven, A. C. (2001) *Proc. Natl. Acad. Sci. U.S.A. 98*, 4328−4333.
38. Moores, C. A., Yu, M., Guo, J., Beraud, C., Sakowicz, R., and Milligan, R. A. (2002) *Mol. Cell 9*, 903−909.
39. Panda, D., DeLuca, K., Williams, D., Jordan, M. A., and Wilson, L. (1998) *Proc. Natl. Acad. Sci. U.S.A. 95*, 9313−9318.

BI020430X